ACS APPLIED MATERIALS & INTERFACES

Research Article

www.acsami.org

Aligned Nanostructured Polymers by Magnetic-Field-Directed Self-Assembly of a Polymerizable Lyotropic Mesophase

Marissa E. Tousley, Xunda Feng, Menachem Elimelech, and Chinedum O. Osuji*

Department of Chemical and Environmental Engineering, Yale University, 9 Hillhouse Avenue, New Haven, Connecticut 06511, United States

Supporting Information

ABSTRACT: Magnetic-field-directed assembly of lyotropic surfactant mesophases provides a scalable approach for the fabrication of aligned nanoporous polymers by templated polymerization. We develop and characterize a lyotropic liquid crystalline system containing hexagonally packed cylindrical micelles of a polymerizable surfactant in a polymerizable solvent. The system exhibits negative magnetic anisotropy, resulting in the degenerate alignment of cylindrical micelles perpendicular to the magnetic field. Sample rotation during field alignment is used to effectively break this degeneracy and enable the production of uniformly well-aligned mesophases. High-fidelity retentions of the hexagonal structure and alignment were successfully achieved in polymer films produced upon UV exposure of the reactive system. The success of this effort provides a route for the fabrication of aligned nanoporous membranes suitable for highly selective separations, sensing, and templated nanomaterial synthesis.

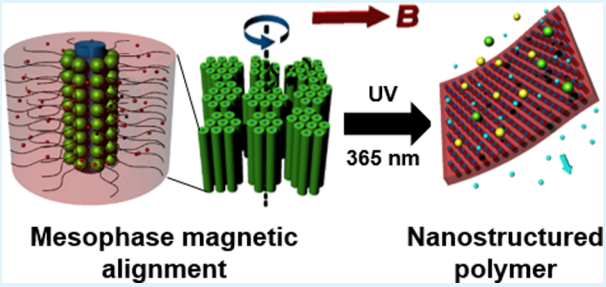

KEYWORDS: *directed self-assembly, nanoporous polymers, lyotropic mesophase, polymer membranes*

INTRODUCTION

Development of functional materials with well-aligned, nanoscale structure is essential for advancement of several transport-based applications, including drug delivery,[1] molecular and chemical sensing,[2,3] catalysis,[4] and membrane separations.[2,5,6] Many materials currently used for these applications suffer from poor control over properties, such as tortuosity and pore size distribution. These limitations are often intrinsic to the methods employed for material fabrication and they adversely affect transport rates, selectivity, and overall process efficiency. For example, achieving highly selective separations with existing commercial micro-, ultra-, or nanofiltration membranes is challenging due to the distribution of pore sizes inherent to membranes formed by conventional techniques.[7] Furthermore, solute transport is hindered by the high tortuosity of these membranes.[8−10]

Lyotropic liquid crystalline mesophases (LLC) provide a promising route for the fabrication of materials with uniform, nanoscale features. They are formed by amphiphilic molecules that self-assemble in the presence of solvent into well-defined supramolecular aggregates with long-range order. A variety of LLC phases can be formed by altering composition and temperature.[11] One approach for transforming these nanostructured gels into mechanically robust functional materials is mesophase polymerization. This is accomplished, for example, through photoinitiated free radical polymerization of mesophases that incorporate reacive monomers and cross-linkers.[12−14] In principle, the polymerization is templated by the structure of the mesophase; however, achieving high-fidelity replication of the template structure in the resulting polymer is incredibly challenging.

Polymerization-induced phase separation between the LLC template and growing polymer chains can alter or completely destroy the original structure.[12,13,15,16] In systems based on nonreactive surfactants, the structure-directing agent does not participate in polymerization and can be easily removed postpolymerization. While successful transfer of LLC order has been achieved in such a system,[17] the resulting polymer only mimics the structure of the template rather than forming an exact replica.[18,19] Polymerization of LLC systems composed of reactive surfactants is generally preferred. In this case, the surfactant serves as both the templating agent and polymer precursor, and the fidelity of the structure templating is significantly better than for the case of nonreactive surfactants.[16,20,21] Compelling examples of functional materials templated from reactive surfactant-based LLC phases and exhibiting promising transport and separation properties have been presented by Gin and co-workers.[22−24]

The inverse hexagonal phase (H_{II}) is a particularly attractive template for functional materials designed for transport applications, as the aqueous cores of the hexagonally packed, cylindrical micelles provide a direct path for ions and molecules to travel. This direct path is in contrast to phases where the pore structure is highly tortuous, such as bicontinuous cubic

Received: July 18, 2014
Accepted: September 2, 2014
Published: September 2, 2014

mesophases.[25] For optimal ionic and molecular transport, however, the randomly oriented H_{II} domains must be aligned with their long axes parallel to the desired transport direction.[26−28] A variety of techniques can be used to achieve alignment, including mechanical shear,[29−32] magnetic fields,[33] and electric fields.[34] Magnetic fields offer the attractive advantages of being space-pervasive, scalable to large areas, and unconstrained by the dielectric breakdown concerns that accompany electric field alignment in many cases.[35] Furthermore, alignment of structures out-of-plane from a substrate or on a microporous support can be readily accomplished.

In LLC systems, magnetic alignment occurs due to anisotropy in the magnetic susceptibilities of aggregate structures, $\Delta\chi = \chi_{\parallel} - \chi_{\perp}$, where $\chi_{\parallel}$ is typically taken as the susceptibility along the long axis of the structure and $\chi_{\perp}$ is the susceptibility perpendicular to the long axis. The additive effects of the anisotropic diamagnetic susceptibilities of individual molecules, when self-assembled into molecular aggregates, are of sufficient magnitude to overcome the disordering forces of Brownian motion at field strengths of a few tesla (T).[36] The effective anisotropic magnetic susceptibility in each molecule arises from a summation of contributions from individual molecular components, including extended aliphatic chains ($\Delta\chi < 0$) and phenyl rings ($\Delta\chi > 0$).[36,37] Due to the high viscosity of LLC phases, molecular motion and aggregate reorientation into thermodynamically preferred states in the presence of a magnetic field is kinetically hindered; however, alignment of LLC phases can be facilitated through appropriate heat treatments dictated by the phase behavior of the system.[38]

Here we report the fabrication of aligned nanostructured polymers, with high-fidelity retention of both templated structure and alignment, by magnetic-field-directed assembly of polymerizable, lyotropic precursors. A schematic illustration of this fabrication scheme is shown in Figure 1. Commercially available, polymerizable, poly(oxyethylenealkylphenyl ether) surfactants were used to form an inverse hexagonal (H_{II}) template containing cylindrical micelles with aqueous cores surrounded by a polymerizable solvent.[39] Through sample rotation and slow cooling across the isotropic−hexagonal transition temperature (T_{iso}) in an applied magnetic field, the template's randomly oriented cylindrical domains were aligned in a nondegenerate fashion perpendicular to the field. Upon photoinitiated polymerization, the template was converted into a nanostructured polymer that retained its alignment and hexagonal order. Aligned nanostructured materials, such as the one presented here, may have implications in the development of size-based separation membranes with enhanced selectivity and transport properties.

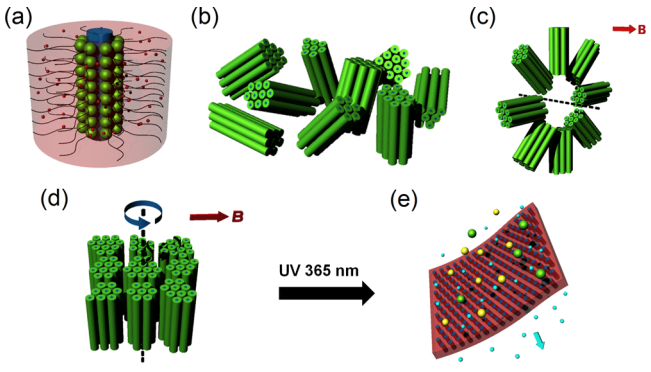

Figure 1. Schematic of aligned porous polymer fabrication from a lyotropic mesophase. The system contains (a) inverse cylindrical micelles formed by self-assembled polymerizable surfactant. Each micelle has an aqueous core and is surrounded by a continuous monomer/cross-linker domain. (b) Domains of hexagonally packed micelles are randomly oriented prior to alignment. (c) The cylindrical domains exhibit an overall negative magnetic anisotropy. Therefore, following magnetic alignment, domains degenerately orient perpendicular to the applied field. (d) Nondegenerate domain orientation can be achieved by sample rotation during magnetic alignment. (e) Following UV exposure, the aligned lyotropic precursor is converted into a porous polymer.

RESULTS AND DISCUSSION

Structure and Phase Behavior. A blend of polymerizable poly(oxyethylenealkylphenyl ether) surfactants, Hitenol BC-05 and Noigen RN-10, in combination with a monomer-based oil phase and water was used in this study to form the H_{II} lyotropic mesophase, as shown in Scheme 1. Prior reported data on a related system[39] was used as a starting point to establish a suitable composition to enable alignment and polymerization. The primary component of the continuous oil phase was *n*-butyl acrylate. 1,4-Butanediol diacrylate, a bifunctional cross-linker, was included in the oil phase to reduce chain mobility and increase structure integrity following polymerization.[16,17] Similar to other lyotropic systems,[16] the phase behavior of this mesophase was sensitive to the amount of cross-linker present, and no more than 1.8% could be incorporated without significantly altering the stability of the H_{II} mesophase. An ultraviolet (UV) photoinitiator was also added to enable UV-initiated polymerization following magnetic alignment. The typical mesophase consisted of 55.3% Hitenol BC-05, 7.90% Noigen RN-10, 17.1% butyl acrylate, 0.95% butanediol diacrylate, 0.95% photoinitiator, and 11.5% water as detailed in the Experimental Section.

Scheme 1. Chemical Structures of Lyotropic Mesophase Components[a]

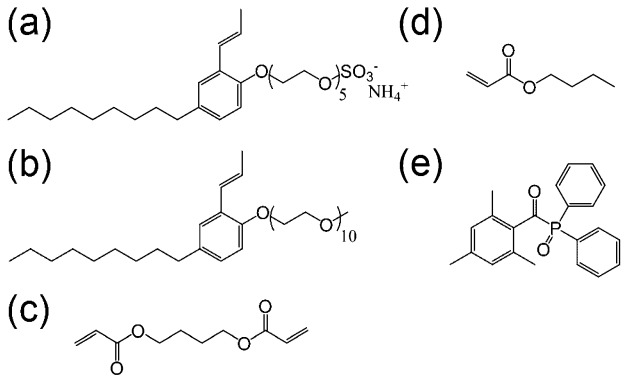

[a](a) Hitenol BC-05; (b) Noigen RN-10; (c) butyl acrylate; (d) butanediol diacrylate; (e) photoinitiator.

Small-angle (SAXS) and wide-angle (WAXS) X-ray scattering were used to confirm the H_{II} ordering of the mesophase (Supporting Information, Figure S1). The primary reflection at $q = 0.135$ Å^{-1} corresponds to a d spacing of 46.5 Å ($d = 2\pi/q$). Higher-order reflections are present at $q = 0.233$ and 0.270 Å^{-1}, exhibiting the characteristic $1:\sqrt{3}:\sqrt{4}$ peak spacing for hexagonal ordering. Figure 2 shows characterization of the mesophase by temperature-resolved polarized optical micros-

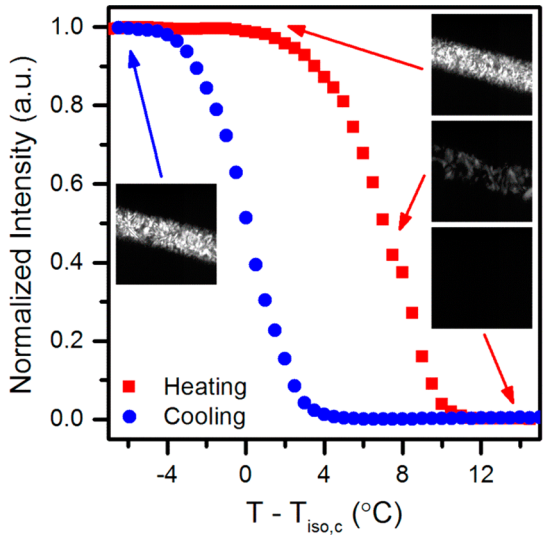

Figure 2. Temperature-resolved polarized optical microscopy (POM) data showing the reversible isotropic transition from H_{II} phase to a disordered micellar state.

copy (POM), where T_{iso} during cooling was selected as a reference point due to its importance in facilitating magnetic alignment over kinetically reasonable time scales.[38] At room temperature, the system exhibits a birefringent, fanlike texture, which is characteristic of hexagonally ordered mesophases.[40] Upon heating above T_{iso}, the system undergoes a reversible transition from the optically anisotropic H_{II} phase to an optically isotropic, disordered micellar state. A corresponding drop in transmitted light intensity is observed in POM due to the lack of birefringence in optically isotropic phases. The temperature of the isotropic transition, T_{iso}, is defined as the inflection point of the transition region. Upon heating, this transition occurs over a temperature range of 10 °C, with $T_{iso,h}$ = 84 °C. Upon cooling, the H_{II} phase reforms and the observed fanlike texture returns over a span of 8 °C, with $T_{iso,c}$ = 77 °C.

Magnetic Field Alignment. Alignment was conducted during passage from the disordered isotropic phase to hexagonally ordered H_{II} phase upon slow cooling across T_{iso} in the presence of a static magnetic field with field strengths ranging from 1 to 6 T. During this process, the surfactant self-assembles into hexagonally packed cylindrical aggregates that adopt a specific orientation with respect to the magnetic field. This thermodynamically preferred orientation is driven by anisotropy in the magnetic susceptibility in the aggregate structures, which arises due to additive effects of diamagnetic susceptibilities of individual molecules.[36]

Figure 3 shows the alignment behavior of the mesophase by use of 2-D SAXS. Samples that have not been aligned display a uniform azimuthal distribution of scattered intensity (Figure 3a,b), which indicates that the cylindrical domains are randomly oriented throughout the system. By contrast, field-processed samples show a nonuniform azimuthal intensity distribution (Figure 3a–c). Samples that are held stationary in the field show a numerous set of reflections, whereas two distinct arcs are observed at azimuthal angles of 90° and 270° for samples that are rotated during the field alignment process. A control experiment where the sample was cooled under rotation in the absence of the field (0 T) resulted in a polycrystalline texture corresponding to randomly oriented grains (Supporting Information, Figure S2). This confirms that the alignment

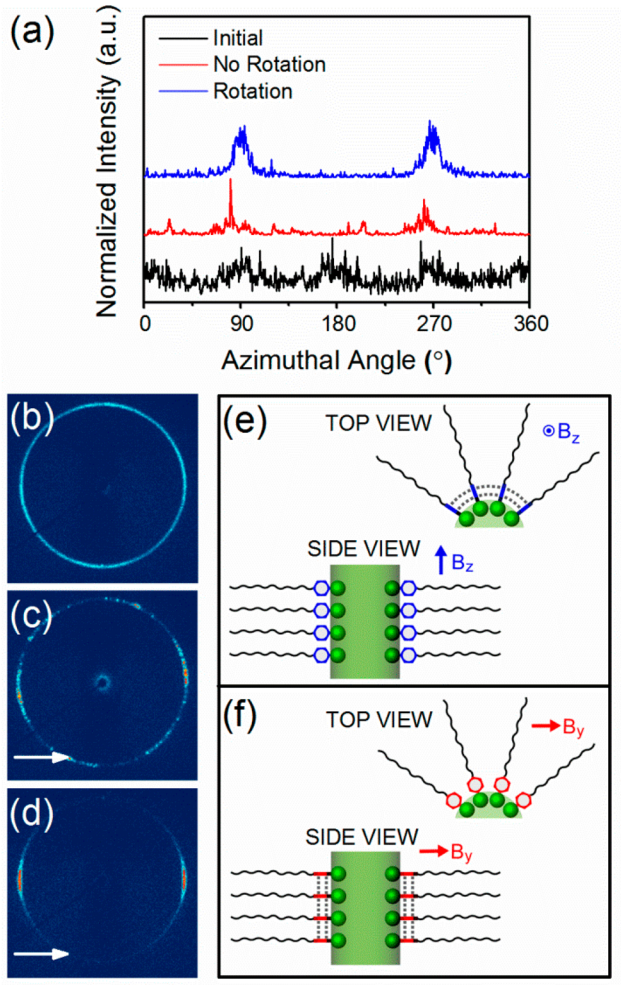

Figure 3. (a) Normalized azimuthal scattering intensity. (b–d) 2-D SAXS of the mesophase, (b) before alignment, (c) after alignment without rotation, and (d) after alignment with rotation. (e, f) Schematics showing possible surfactant orientations during alignment: (e) circumferential stacking, where π–π stacking may be constrained by curvature, and (f) cylindrical long-axis stacking, where π–π stacking is not constrained.

observed for field-processed samples was indeed driven by the magnetic field and not by any surface effects from the glass capillary encapsulating the system.

The scattering data of field-aligned samples are consistent with the formation of degenerately aligned structures for the stationary sample (Figure 3c), and nondegenerately aligned structures for the rotated case (Figure 3d).[41] The concentration of scattered intensity along the equatorial direction, parallel to the magnetic field direction, signals that the lattice vector is parallel to the field. This, in turn, indicates that the long axes of the cylindrical aggregates themselves are perpendicular to the field, implying that the cylindrical domains have a negative magnetic anisotropy. Uniaxial species, such as cylindrical domains, possessing a negative magnetic anisotropy are well-known to have a degeneracy inherent in the alignment, which can be broken through sample rotation to impose a unique orientation of the structure.[41,42] Given the perpendicular orientation of the long axis of the surfactants with respect to the perpendicularly oriented cylinders, we can deduce that these individual species possess a positive molecular magnetic anisotropy.

We speculate that the system anisotropy is due to dominant contributions from the π bonding orbitals of both the phenyl ring and the unsaturated vinyl group in-plane with the aromatic group in the polymerizable surfactants.[43−45] It is possible that $\pi-\pi$ stacking interactions also play a role, where packing constraints associated with circumferential stacking of the phenyl rings may influence surfactant self-assembly, even in the absence of the field.[39,46] The molecular orientation shown in Figure 3e would permit the simultaneous preferred perpendicular alignment of the alkyl groups and parallel alignment of the phenyl ring to the magnetic field; however, $\pi-\pi$ interactions along the circumference of the cylindrical micelle would be severely constrained by curvature. By contrast, $\pi-\pi$ interactions parallel to the micelle long axis are not curvature-constrained (Figure 3f), but such an arrangement does not permit simultaneous preferred alignment of the molecular segments. These aspects were not further considered as they were beyond the scope of the present study.

We examined the evolution of alignment as a function of temperature while cooling at 0.1 °C/min through the transition region from an isotropic to hexagonally ordered state, under rotation at a field strength of 6 T. Alignment appears to occur simultaneously with structure formation. That is, the first visible scattering from the H_{II} mesophase is anisotropic, indicating alignment of the cylindrical aggregates by the field as they form (Figure 4). Further cooling to room temperature ($T - T_{iso,c}$ = −38 °C) results in an increase in scattered intensity and a slight narrowing of the azimuthal intensity distribution. This is in contrast to the situation observed in a field-aligned block copolymer, where randomly oriented structures are first nucleated and thereafter slowly rotate to align with the field.[47] The disparity suggests that the magnetic field alters the lyotropic phase equilibrium enough to bias the system toward aligned nucleation and growth, rather than random nucleation and grain rotation. It should be noted that the width of the order−disorder transition region in SAXS is greater than that measured in POM. This observation is due to a systematic difference between the temperature control systems of the POM and SAXS heating stages. In the latter case, thermal contact between the sample and heating stage is compromised by the mechanism that facilitates sample rotation in the field while under X-ray observation.

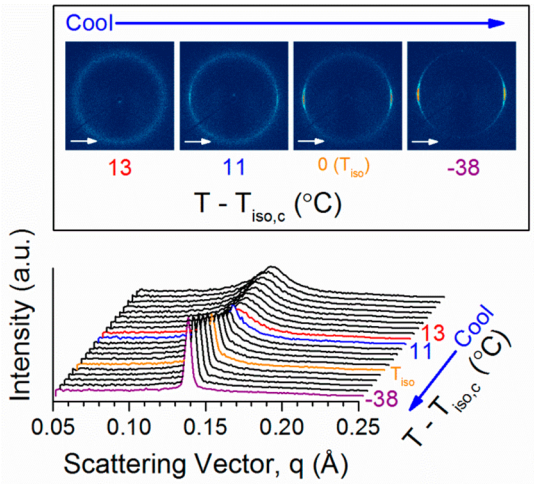

Figure 4. SAXS data showing structure formation and evolution of alignment while cooling at 0.1 °C/min through the isotropic transition region in a 6 T magnetic field. 2-D SAXS data correspond to labeled points in the 1-D waterfall plot.

The influence of magnetic field strength on alignment during rotation was investigated. Highly aligned samples were achieved at both 5 and 6 T field strengths, as evidenced by the well-defined peaks in the azimuthal intensity distributions (Figure 5a). The full width at half-maximum (fwhm) values of the peaks are 19.8° and 19.3° for the 5 and 6 T field strengths, respectively, as measured by Guassian fits of the azimuthal intensity variation. From this data, we calculate an orientational order parameter, $\langle P_2 \rangle$, which is the coefficient of the second Legendre polynomial describing the orientation distribution.[48] At both 5 and 6 T, $\langle P_2 \rangle$ = 0.94. The alignment quality declines noticeably, however, upon decreasing the magnetic field strength to 4 T. At this field strength the fwhm was 84.8° with $\langle P_2 \rangle$ = 0.36. No alignment of the system could be reliably discerned from samples aligned at 2 T. A decrease in alignment quality with decreasing field strength has previously been reported for other lyotropic and block copolymer systems.[35,42] The mesophase discussed here requires higher field strengths for alignment than some single-tailed surfactant lyotropics of comparable molecular weight.[42] This may be due to a smaller anisotropy in the diamagnetic susceptibility of the molecular aggregates or to a higher viscosity of the mesophase. In the former case, competing contributions to the net diamagnetic susceptibility of individual molecules, arising from negative

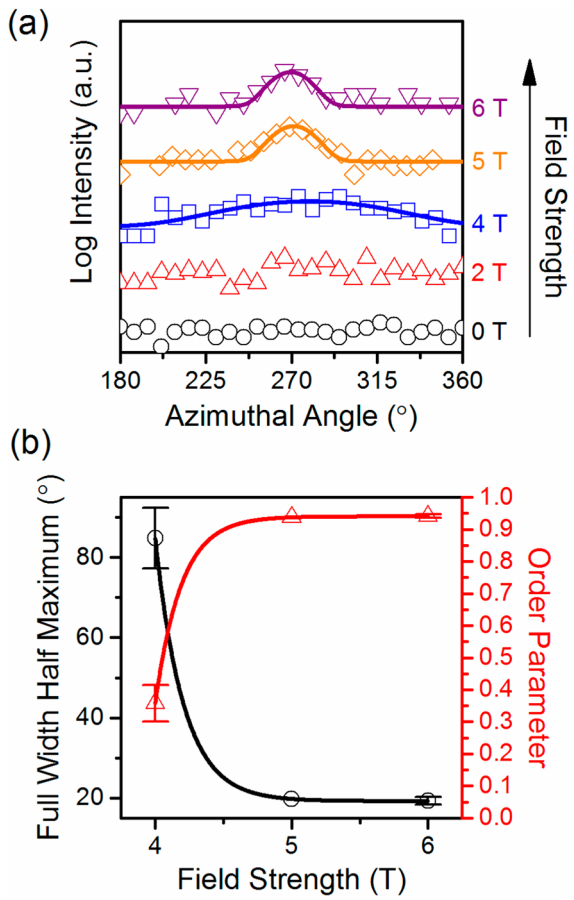

Figure 5. (a) SAXS scattering intensity as a function of azimuthal angle at different magnetic field strengths. Solid lines are Gaussian fits. (b) Full width at half-maximum (fwhm) and order parameter ($\langle P \rangle$) as a function of magnetic field strength. Solid lines are a guide to the eye.

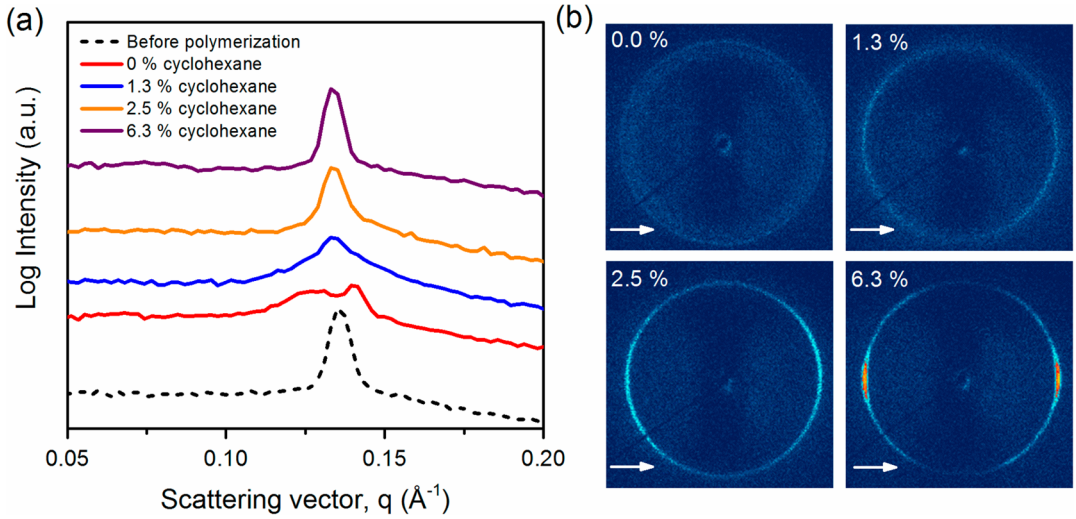

Figure 6. (a) 1-D SAXS data showing structure retention; (b) 2-D SAXS patterns showing alignment retention of polymerized samples doped with cyclohexane. Total percent of cyclohexane within the system is reported. Prior to polymerization, samples were aligned in a 6 T magnetic field.

anisotropy of the alkyl chain and positive anisotropy of the phenyl group, could lead to lower anisotropy in the aggregate diamagnetic susceptibility.[36,43]

Polymerization of Aligned Mesophase. Following nondegenerate magnetic alignment, the system was polymerized to render a polymer potentially suitable for transport applications. Prior to polymerization, the structure and stability of the mesophase is highly susceptible to changes in composition and temperature. Initially, polymerization of mesophase with an oil phase containing only monomer, cross-linker, and initiator was investigated. Isotropic scattering and splitting of the first-order peak is observed by SAXS, indicating loss of structure due to phase separation of forming polymer chains from the rest of the mesophase (Figure 6). Poor kinetics during the polymerization reaction is one potential cause of this observed phase separation. While adjustments to photoinitiator content, temperature, and air versus nitrogen atmosphere were made in an attempt to optimize kinetics, the most substantial improvement to structure retention following system polymerization was achieved through addition of a small amount of nonreactive species to the oil phase. By doping the system with 1.3% cyclohexane, a single, as opposed to a split, first-order scattering peak is observed in SAXS following polymerization. This peak is wider and has lower intensity than the scattering peak prior to polymerization, but some H_{II} ordering must still be preserved. A decrease in scattering peak width and an increase in intensity in polymerized systems containing 2.5% cyclohexane indicate improved structure retention; however, the isotropic intensity in 2-D SAXS shows that alignment retention is still insignificant. Upon further increasing the amount of cyclohexane in the system to 6.3%, the system displays anisotropic scattering, signifying the retention of both structure and alignment. The location of the first-order peak is slightly shifted to q = 0.132 Å^{-1} and a d spacing of 47.6 Å. Structure retention was further confirmed by preservation of the second- and third-order H_{II} phase reflections in WAXS for an unaligned, polymerized sample containing 6.3% cyclohexane (Supporting Information, Figure S1).

The presence of nonreactive oil species, such as cyclohexane, is believed to help maintain the effective hydrophobic chain volume needed for H_{II} phase stability.[49] During polymerization, spacing between the surfactant molecules shrinks near the oil–water interface due to cross-linking of the vinyl groups. This shrinking changes the packing parameter, a metric of preferred aggregate geometry, and destabilizes the inverted cylinders in favor of lower-curvature geometries. Nonreactive oil species in the mesophase can penetrate into the hydrophobic chains and stabilize the effective volume during polymerization, such that the packing parameter remains suitable for H_{II} structure retention.[49]

Polymerization of the mesophase with 6.3% cyclohexane doping produces a free-standing polymer with aligned nanostructure. The geometry of the resulting material is dictated by the vessel confining the mesophase prior to photopolymerization and can be engineered for the desired application. For example, a film (Figure 7) would be of suitable

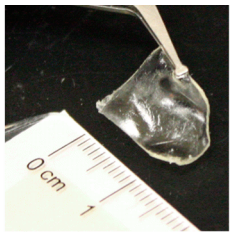

Figure 7. Photograph of polymerized mesophase.

geometry for size-based separation membranes. The polymer film pictured is non-water-soluble and after several days stored in water shows no visible signs of degradation. Based on the known mesophase composition ($\varnothing_{water}$ = 11.3%) and scattering data (d = 4.76 nm), the average pore size of such a polymer film is estimated to be 2 nm in diameter ($\varnothing_w = \sqrt{3\pi r_w^2/2d^2}$, where r_w is the radius of the water channel).[39]

CONCLUSIONS

We have developed a H_{II} LLC system that can be magnetically aligned and photopolymerized to produce out-of-plane, aligned nanoporous polymers, including films. Sample rotation during magnetic field processing was successfully used to achieve nondegenerate alignment of the mesophase. Alignment was characterized through temperature- and field-dependent

studies. The use of a nonreactive, oil-based dopant was shown to enable retention of H_{II} structure and alignment following polymerization. This work provides a platform suitable for the development and scalable fabrication of aligned nanoporous films, which may have application in tight molecular weight cutoff separations. The low-tortuosity monodisperse nanostructures in the polymers fabricated here have the potential to enhance size-based separation membrane transport and selectivity, overcoming two of the performance-limiting characteristics intrinsic to existing membrane materials.

EXPERIMENTAL SECTION

Materials. Polymerizable poly(oxyethylenealkylphenyl ether) surfactants Hitenol BC-05 and Noigen RN-10 were obtained from Montello Inc. (Tulsa, OK). Butyl acrylate (99%), 1,4-butanediol-diacrylate (90%), diphenyl(2,4,6-trimethylbenzoyl)phosphine oxide (photoinitiator, 97%), cyclohexane (ACS reagent, 99%), and cyclooctane (99%) were purchased from Sigma–Aldrich and used as received. Ultrapure water was obtained from a Millipore Milli-Q system.

Lyotropic Template Preparation. Mesophases were prepared in approximately 3 g batches of the following composition: 63.2% surfactant blend (1.896 g), 25.3% oil stock (0.759 g), and 11.5% water (0.345 mL). This composition was selected after a thorough study of phase stability, alignment quality, and polymerization behavior. The surfactant blend and oil stock were mixed prior to the addition of water. The mesophase was then homogenized by vortexing, centrifugation, and gentle heating. The surfactant blend used in mesophase preparation contained a 7:1 weight ratio of Hitenol BC-05 and Noigen RN-10. A standard oil stock containing 67.5% butyl acrylate, 3.75% butanediol diacrylate, 3.75% photoinitiator, and 25% cyclohexane or cyclooctane was prepared prior to mesophase preparation and used for polymerization experiments. Initiator was omitted from the oil phase for characterization of the order–disorder transition temperature and semi-isothermal alignment experiments in order to prevent polymerization during measurements. A base oil solution of 90% butyl acrylate, 5% butanedioldiacrylate, and 5% photoinitiator was used for the 0% case in the cyclohexane doping experiments. This base solution was subsequently combined with the necessary amount of cyclohexane to form the oil phases used in the 5%, 10%, and 25% doping cases, where doping percent refers to the percent of cyclohexane in the oil phase. Due to the slight shift in phase behavior with cyclohexane addition, the 0% and 5% doped mesophases were prepared with a 2.25:1 rather than a 2.5:1 surfactant/oil ratio.

X-ray Scattering. Small-angle X-ray scattering (SAXS) was performed on a Rigaku SMax-3000 with pinhole-collimated Cu Kα radiation (λ = 1.542 Å). A 2-D electronic wire detector was used to record SAXS patterns for a scattering vector (q) range of 0.02–0.22 $Å^{-1}$. Wide-angle X-ray scattering (WAXS) was performed on a Rigaku 007 HF+ with a rotating-anode Cu Kα X-ray source and a 2-D Saturn 994+ charge-coupled device (CCD) detector. Silver behenate, with a d spacing of 58.38 Å, was used for data calibration. Azimuthal averaging was carried out via Matlab routines (Rigaku) to integrate 2-D scattering patterns into 1-D plots of intensity (I) versus q, where $q = (4\pi/\lambda)\sin\theta$ and the scattering angle is 2θ.

For phase characterization, the hexagonal system was sandwiched between two kapton sheets and measured by SAXS for 30 min. For all other scattering experiments, sample preparation involved placing mesophase into a 1.5 mm inner diameter glass capillary with one flame-sealed end, by use of a needle attached to a syringe. The capillary was then centrifuged to remove bubbles. Immediately after centrifugation, the open end of the capillary was sealed with 5 min epoxy (ITW Devcon, Danvers, MI); extra care was taken to minimize open head space. After the epoxy was allowed to set for 5–10 min, the epoxy-sealed end of the capillary was placed and centered in an epoxy-filled 2.5 mm i.d. aluminum tube. The aluminum tube was necessary for placement in our custom SAXS rotary sample holder and also provided an additional level of capillary sealing. Temperature-resolved SAXS data were collected on an Omega CN8202 controller. For characterization of T_{iso}, samples were heated at 0.5 °C/min to 110 °C and then cooled at 0.5 °C/min, except around the transition region where samples were cooled at 0.2 °C/min. Prior to 10 min SAXS acquisition at different temperature points, samples were allowed to equilibrate for 3 min. For cyclohexane doping and polymerization experiments, SAXS was collected for 15 min. WAXS measurements were based on the average of two 20-min collections.

Order parameters were calculated as a function of full width at half-maximum (fwhm) from a Gaussian fit of the azimuthal data. Fits were made to each half of the azimuthal data separately (i.e., 0–180° and 180–360°) and the two fwhm were averaged. The relation used was derived from eq 1 following integration in Mathematica, where θ is the azimuthal angle.

$$\langle P_2(\cos\theta)\rangle = \frac{\int_0^{\pi/2} I(q,\theta)\frac{(3\cos\theta^2-1)}{2}\sin\theta\,\mathrm{d}\theta}{\int_0^{\pi/2} I(q,\theta)\sin\theta\,\mathrm{d}\theta} \quad (1)$$

Polarized Optical Microscopy. POM was conducted on a Zeiss Axio Observer microscope equipped with a Pike CCD camera. For phase studies, samples were placed between two glass slides. Birefringent texture was observed immediately after sample preparation and after approximately 10 min of equilibration. Temperature-resolved measurements were carried out at a 1 °C/min heating and cooling rate by use of a Linkam THMS600 hot stage. Mesophase was flame-sealed in a glass capillary for each measurement. The average intensity of recorded images was extracted via a Matlab code and plotted as a function of temperature for determination of T_{iso}.

Magnetic Alignment. Magnetic alignment of the lyotropic system was carried out with a superconducting electromagnet (American Magnetics Inc.) held at a 6 T static field. Samples were sealed in glass capillaries mounted in aluminum tubes, as described above, to enable placement in our rotary setup. Samples were rotated at 6.75 rpm during alignment, except for "no rotation" experiments where samples were stationary. For polymerization experiments, samples were heated to 115 °C and held for 5 min to disorder the structure. Samples were then cooled at 3 °C/min to 100 °C, at 0.3 °C/min to 60 °C, at 0.5 °C/min to 50 °C, and at 2.5 °C/min to 25 °C. This stepwise cooling protocol was designed to restrict slow cooling to only the isotropic transition region and minimize time at high temperature in order to avoid template polymerization during the alignment process. For semi-isothermal alignment experiments with in situ SAXS collection, samples underwent the same heat treatment as described for collection of SAXS T_{iso} data; however, a cooling rate of 0.1 °C/min was used within the transition region.

Template Polymerization and Polymer Characterization. Mesophase polymerization was carried out by use of a 365 nm UV lamp with an intensity of 500 $\mu W/cm^2$ (UVP, Upland, CA). Samples were sealed in round or rectangular glass capillaries and placed at a distance of 5.5 cm from the lamp. Larger films were prepared by sandwiching mesophase between two mylar sheets separated by a 0.4 mm double-sided tape spacer. Quartz slides were placed on top of the mylar sheets and held together with mini binder clips.

ASSOCIATED CONTENT

Supporting Information

Two figures showing X-ray scattering confirming H_{II} phase and 2-D SAXS after heat treatment in a 0 T magnetic field. This material is available free of charge via the Internet at http://pubs.acs.org.

AUTHOR INFORMATION

Corresponding Author

*E-mail chinedum.osuji@yale.edu; phone 203-432-4347.

Notes

The authors declare no competing financial interest.

■ ACKNOWLEDGMENTS

This material is based upon work supported by the National Science Foundation under Grant CBET-1133484 and Graduate Research Fellowship DGE-1122492 awarded to M.E.T. Any opinion, findings, and conclusions or recommendations expressed in this material are those of the authors and do not necessarily reflect the views of the National Science Foundation. We thank Youngwoo Choo, Dr. Pawel Majewski, and Dr. Manesh Gopinadhan for useful discussions on scattering and magnetic alignment in microscopic imaging. We also thank Dr. Brandon Mercado of the Chemical and Biophysical Instrumentation Center at Yale University for assistance with WAXS measurements.

■ REFERENCES

(1) Drummond, C. J.; Fong, C. Surfactant Self-Assembly Objects as Novel Drug Delivery Vehicles. *Curr. Opin. Colloid Interface Sci.* **1999**, *4*, 449−456.
(2) Bohn, P. W. Nanoscale Control and Manipulation of Molecular Transport in Chemical Analysis. *Annu. Rev. Anal. Chem.* **2009**, *2*, 279−296.
(3) Kolmakov, A.; Moskovits, M. Chemical Sensing and Catalysis by One-Dimensional Metal-Oxide Nanostructures. *Annu. Rev. Mater. Res.* **2004**, *34*, 151−180.
(4) Shiju, N. R.; Guliants, V. V. Recent Developments in Catalysis Using Nanostructured Materials. *Appl. Catal., A* **2009**, *356*, 1−17.
(5) Jackson, E. A.; Hillmyer, M. A. Nanoporous Membranes Derived from Block Copolymers: From Drug Delivery to Water Filtration. *ACS Nano* **2010**, *4*, 3548−3553.
(6) Phillip, W. A.; Mika Dorin, R.; Werner, J. R.; Hoek, E. M. V.; Wiesner, U.; Elimelech, M. Tuning Structure and Properties of Graded Triblock Terpolymer-Based Mesoporous and Hybrid Films. *Nano Lett.* **2011**, *11*, 2892−2900.
(7) Strathmann, H.; Kock, K. The Formation Mechanism of Phase Inversion Membranes. *Desalination* **1977**, *21*, 241−255.
(8) Dullien, F. A. *Porous Media: Fluid Transport and Pore Structure*; Academic Press: San Diego, CA, 1991.
(9) Song, X.; Liu, Z.; Sun, D. D. Nano Gives the Answer: Breaking the Bottleneck of Internal Concentration Polarization with a Nanofiber Composite Forward Osmosis Membrane for a High Water Production Rate. *Adv. Mater.* **2011**, *23*, 3256−3260.
(10) Tiraferri, A.; Yip, N. Y.; Phillip, W. A.; Schiffman, J. D.; Elimelech, M. Relating Performance of Thin-Film Composite Forward Osmosis Membranes to Support Layer Formation and Structure. *J. Membr. Sci.* **2011**, *367*, 340−352.
(11) Mezzenga, R. Physics of Self-Assembly of Lyotropic Liquid Crystals. In *Self-Assembled Supramolecular Architectures: Lyotropic Liquid Crystals*; Garti, N., Somasundaran, P., Mezzenga, R., Eds.; John Wiley & Sons: Hoboken, NJ, 2012; Chapt. 1, pp 1−20.
(12) Antonietti, M.; Caruso, R. A.; Göltner, C. G.; Weissenberger, M. C. Morphology Variation of Porous Polymer Gels by Polymerization in Lyotropic Surfactant Phases. *Macromolecules* **1999**, *32*, 1383−1389.
(13) DePierro, M. A.; Carpenter, K. G.; Guymon, C. A. Influence of Polymerization Conditions on Nanostructure and Properties of Polyacrylamide Hydrogels Templated from Lyotropic Liquid Crystals. *Chem. Mater.* **2006**, *18*, 5609−5617.
(14) McCormick, D. T.; Stovall, K. D.; Guymon, C. A. Photopolymerization in Pluronic Lyotropic Liquid Crystals: Induced Mesophase Thermal Stability. *Macromolecules* **2003**, *36*, 6549−6558.
(15) Antonietti, M.; Hentze, H. P. Synthesis of Sponge-Like Polymer Dispersions Via Polymerization of Bicontinuous Microemulsions. *Colloid Polym. Sci.* **1996**, *274*, 696−702.
(16) Sievens-Figueroa, L.; Guymon, C. A. Cross-Linking of Reactive Lyotropic Liquid Crystals for Nanostructure Retention. *Chem. Mater.* **2009**, *21*, 1060−1068.
(17) Zhang, J.; Xie, Z.; Hill, A. J.; She, F. H.; Thornton, A. W.; Hoang, M.; Kong, L. X. Structure Retention in Cross-Linked Poly(ethylene glycol) Diacrylate Hydrogel Templated from a Hexagonal Lyotropic Liquid Crystal by Controlling the Surface Tension. *Soft Matter* **2012**, *8*, 2087−2094.
(18) Clapper, J. D.; Guymon, C. A. Physical Behavior of Cross-Linked Peg Hydrogels Photopolymerized within Nanostructured Lyotropic Liquid Crystalline Templates. *Macromolecules* **2007**, *40*, 1101−1107.
(19) Hulvat, J. F.; Stupp, S. I. Liquid-Crystal Templating of Conducting Polymers. *Angew. Chem., Int. Ed.* **2003**, *42*, 778−781.
(20) Srisiri, W.; Sisson, T. M.; O'Brien, D. F.; McGrath, K. M.; Han, Y.; Gruner, S. M. Polymerization of the Inverted Hexagonal Phase. *J. Am. Chem. Soc.* **1997**, *119*, 4866−4873.
(21) Pindzola, B. A.; Hoag, B. P.; Gin, D. L. Polymerization of a Phosphonium Diene Amphiphile in the Regular Hexagonal Phase with Retention of Mesostructure. *J. Am. Chem. Soc.* **2001**, *123*, 4617−4618.
(22) Zhou, M.; Nemade, P. R.; Lu, X.; Zeng, X.; Hatakeyama, E. S.; Noble, R. D.; Gin, D. L. New Type of Membrane Material for Water Desalination Based on a Cross-Linked Bicontinuous Cubic Lyotropic Liquid Crystal Assembly. *J. Am. Chem. Soc.* **2007**, *129*, 9574−9575.
(23) Bara, J. E.; Kaminski, A. K.; Noble, R. D.; Gin, D. L. Influence of Nanostructure on Light Gas Separations in Cross-Linked Lyotropic Liquid Crystal Membranes. *J. Membr. Sci.* **2007**, *288*, 13−19.
(24) Carter, B. M.; Wiesenauer, B. R.; Hatakeyama, E. S.; Barton, J. L.; Noble, R. D.; Gin, D. L. Glycerol-Based Bicontinuous Cubic Lyotropic Liquid Crystal Monomer System for the Fabrication of Thin-Film Membranes with Uniform Nanopores. *Chem. Mater.* **2012**, *24*, 4005−4007.
(25) Wiesenauer, B. R.; Gin, D. L. Nanoporous Polymer Materials Based on Self-Organized, Bicontinuous Cubic Lyotropic Liquid Crystal Assemblies and Their Applications. *Polym. J.* **2012**, *44*, 461−468.
(26) Majewski, P. W.; Gopinadhan, M.; Osuji, C. O. Understanding Anisotropic Transport in Self-Assembled Membranes and Maximizing Ionic Conductivity by Microstructure Alignment. *Soft Matter* **2013**, *9*, 7106−7116.
(27) Huang, Y.; Cong, Y.; Li, J.; Wang, D.; Zhang, J.; Xu, L.; Li, W.; Li, L.; Pan, G.; Yang, C. Anisotropic Ionic Conductivities in Lyotropic Supramolecular Liquid Crystals. *Chem. Commun.* **2009**, 7560−7562.
(28) Vallooran, J. J.; Negrini, R.; Mezzenga, R. Controlling Anisotropic Drug Diffusion in Lipid-Fe_3O_4 Nanoparticle Hybrid Mesophases by Magnetic Alignment. *Langmuir* **2013**, *29*, 999−1004.
(29) Schmidt, G.; Müller, S.; Lindner, P.; Schmidt, C.; Richtering, W. Shear Orientation of Lyotropic Hexagonal Phases. *J. Phys. Chem. B* **1998**, *102*, 507−513.
(30) Seddon, A. M.; Lotze, G.; Plivelic, T. S.; Squires, A. M. A Highly Oriented Cubic Phase Formed by Lipids under Shear. *J. Am. Chem. Soc.* **2011**, *133*, 13860−13863.
(31) Liu, L.; Singh, M.; John, V. T.; McPherson, G. L.; He, J.; Agarwal, V.; Bose, A. Shear-Induced Alignment and Nanowire Silica Synthesis in a Rigid Crystalline Surfactant Mesophase. *J. Am. Chem. Soc.* **2004**, *126*, 2276−2277.
(32) Singh, M.; Agarwal, V.; De Kee, D.; McPherson, G.; John, V.; Bose, A. Shear-Induced Orientation of a Rigid Surfactant Mesophase. *Langmuir* **2004**, *20*, 5693−5702.
(33) Forrest, B. J.; Reeves, L. W. New Lyotropic Liquid Crystals Composed of Finite Nonspherical Micelles. *Chem. Rev.* **1981**, *81*, 1−14.
(34) Thurn-Albrecht, T.; DeRouchey, J.; Russell, T. P.; Jaeger, H. M. Overcoming Interfacial Interactions with Electric Fields. *Macromolecules* **2000**, *33*, 3250−3253.
(35) Majewski, P. W.; Gopinadhan, M.; Osuji, C. O. Magnetic Field Alignment of Block Copolymers and Polymer Nanocomposites: Scalable Microstructure Control in Functional Soft Materials. *J. Polym. Sci., Part B: Polym. Phys.* **2012**, *50*, 2−8.
(36) Firouzi, A.; Schaefer, D. J.; Tolbert, S. H.; Stucky, G. D.; Chmelka, B. F. Magnetic-Field-Induced Orientational Ordering of Alkaline Lyotropic Silicate-Surfactant Liquid Crystals. *J. Am. Chem. Soc.* **1997**, *119*, 9466−9477.

(37) Rapp, A.; Ermolaev, K.; Fung, B. M. The Alignment of Lyotropic Liquid Crystals Formed by Hexadecyltrimethylammonium Bromide in D_2O in a Magnetic Field. *J. Phys. Chem. B* **1999**, *103*, 1705−1711.
(38) Tolbert, S. H.; Firouzi, A.; Stucky, G. D.; Chmelka, B. F. Magnetic Field Alignment of Ordered Silicate-Surfactant Composites and Mesoporous Silica. *Science* **1997**, *278*, 264−268.
(39) Mauter, M. S.; Elimelech, M.; Osuji, C. O. Stable Sequestration of Single-Walled Carbon Nanotubes in Self-Assembled Aqueous Nanopores. *J. Am. Chem. Soc.* **2012**, *134*, 3950−3953.
(40) Hyde, S. T., Identification of Lyotropic Liquid Crystalline Mesophases. In *Handbook of Applied Surface and Colloid Chemistry*, Holmberg, K., Ed.; Wiley: New York, 2001; Chapt. 16, pp 299−332.
(41) Majewski, P. W.; Osuji, C. O. Non-Degenerate Magnetic Alignment of Self-Assembled Mesophases. *Soft Matter* **2009**, *5*, 3417−3421.
(42) Majewski, P. W.; Osuji, C. O. Controlled Alignment of Lamellar Lyotropic Mesophases by Rotation in a Magnetic Field. *Langmuir* **2010**, *26*, 8737−8742.
(43) Lonsdale, K. Diamagnetic Anisotropy of Organic Molecules. *Proc. R. Soc. London, Ser. A* **1939**, *171*, 541−568.
(44) Jeu, W. H. The Magnetic Susceptibility. In *Physical Properties of Lyotropic Liquid Crystalline Materials*; Grey, G., Ed.; Gordon and Breach: New York, 1980; Chapt. 3, pp 24−33.
(45) Lonsdale, K. Magnetic Anisotropy and Electronic Structure of Aromatic Molecules. *Proc. R. Soc. London, Ser. A* **1937**, *159*, 149−161.
(46) Janiak, C. A Critical Account on $\pi-\pi$ Stacking in Metal Complexes with Aromatic Nitrogen-Containing Ligands. *Dalton (2000)* **2000**, 3885−3896.
(47) Gopinadhan, M.; Majewski, P. W.; Choo, Y.; Osuji, C. O. Order-Disorder Transition and Alignment Dynamics of a Block Copolymer under High Magnetic Fields by in Situ X-Ray Scattering. *Phys. Rev. Lett.* **2013**, *110*, No. 078301.
(48) Tran, H.; Gopinadhan, M.; Majewski, P. W.; Shade, R.; Steffes, V.; Osuji, C. O.; Campos, L. M. Monoliths of Semiconducting Block Copolymers by Magnetic Alignment. *ACS Nano* **2013**, *7*, 5514−5521.
(49) Israelachvili, J. N. Soft and Biological Structures. In *Intermolecular and Surface Forces*, 3rd ed.; Israelachvili, J. N., Ed.; Academic Press: San Diego, CA, 2011; pp 535−576.